Journal of Catalysis **189,** 382–394 (2000)
doi:10.1006/jcat.1999.2718, available online at http://www.idealibrary.com on IDEAL®

Determination of the Pore Topology of Zeolite IM-5 by Means of Catalytic Test Reactions and Hydrocarbon Adsorption Measurements

A. Corma,*,[1] A. Chica,* J. M. Guil,† F. J. Llopis,‡ G. Mabilon,§ J. A. Perdigón-Melón,* and S. Valencia*

*Instituto de Tecnología Química (UPV-CSIC), Universidad Politécnica de Valencia, Avda. de los Naranjos, s/n, 46022 Valencia, Spain; †Instituto de Química-Física Rocasolano (CSIC), Serrano, 117, 28006 Madrid, Spain; ‡Departmento de Ingeniería Química, Universitat de Valencia, 46100 Burjassot, Spain; and §Institut Français du Pétrole, 1 et 4 avenue des Bois-Préau, B.P. 311, 92506 Rueil, Malmaison Cedex, France

Received June 10, 1999; revised October 1, 1999; accepted October 5, 1999

The pore topology of a recently synthesized zeolite IM-5 has been determined by means of catalytic test reactions, i.e., *n*-decane hydroisomerization–cracking, *m*-xylene isomerization–disproportionation, *n*-hexadecane isodewaxing, and adsorption–microcalorimetry of molecules with different sizes and shapes (*n*-hexane, toluene, *m*-xylene, and 1,3,5 trimethylbenzene). It has been found that the channel network consists of a system of unidirectional 10 MR with lobes or side pockets, or crossing 10 membered ring pores with a pore diameter somewhat smaller than those in ZSM-5. This structure offers interesting shape selectivity features for catalytic reactions. © 2000 Academic Press

Key Words: **IM-5 zeolite; pore topology; IM-5 catalytic activity; IM-5 adsorption properties.**

1. INTRODUCTION

The search for new shape selectivity effects has motivated researchers to work in particular toward the synthesis of new bidimensional 10-membered ring (MR) zeolite structures as well as new zeolitic materials which have pores with different diameters. In the first case, achieving bidimensional 10 MR zeolites with pore dimensions and topologies different from those of ZSM-5 could certainly expand the successful shape selectivity already shown by the MFI and MEL structures. Unfortunately, up to now and as far as we know, no new structures of the type described above have been discovered. More success, however, has been achieved in the synthesis of zeolites with structures which simultaneously contain 10 and 12 MR pores. Zeolites have been synthesized which either cross as in SSZ-26 and NU-87 (1, 2), are independent (MWW) (3), or which combine 10, 11, and 12 MR pores in the same structure as in NU-86 (4).

Recently (5), a new zeolite that presents a pore volume of 0.13 $cm^3\ g^{-1}$, having an unknown structure (IM-5), was synthesized. When this pore volume is compared with those of uni- and bidirectional 10 MR, uni- and tridirectional 12 MR, and 10 × 12 MR zeolites (Table 1), it appears that this zeolite may fall into the porosity range of interest for shape selectivity.

Determination of the structure will certainly help to rationalise both adsorption and catalytic results and also to permit potential uses for this particular zeolite as a selective catalyst in the fields of oil refining, petrochemistry, and chemical production. Physical techniques such as XRD and neutron and electron diffraction are the most adequate tools to determine the crystalline structure of molecular sieves. However, despite recent advances, the determination of zeolite structures by the above techniques is not a simple task. Nevertheless, a good approximation of the pore topology of molecular sieves can be obtained by adsorbing and reacting well-selected probe molecules (6–9). While adsorption and reactivity studies cannot give details on the crystalline structure, they can be of special interest since they indicate how the chosen molecules "see" that particular structure.

In this paper we will present the synthesis of IM-5 together with adsorption and reactivity studies directed specially toward gaining information on the pore topology of this new structure.

2. EXPERIMENTAL

Synthesis of IM-5

The crystallisation of IM-5 (5) was carried out in static conditions at 448 K in PTFE-lined stainless steel 60-ml autoclaves. The organic structure-directing agent employed was 1,5-bis(methylpyrrolidinium)pentane in its bromide form (R) which was synthesised starting from 1-methylpyrrolidine and 1,5-dibromopentane in acetone as the solvent under refluxed conditions.

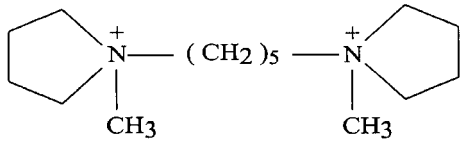

(R)

[1] To whom correspondence should be addressed. Fax: 34963877809. E-mail: acorma@itq.upv.es.

0021-9517/99 $35.00

TABLE 1

Pore Volume and Topology of Different Zeolites

Zeolite	Topology	Pore volume ($cm^3\ g^{-1}$)
ZSM-22	10 MR	0.10
ZSM-48	10 MR	0.11
Ferrierite	10×8	0.11
ZSM-5	10×10	0.12
ZSM-12	12 MR	0.12
SSZ-24	12 MR	0.12
SSZ-26	12×10	0.19
Mordenite	12×8	0.15
MCM-22	$10 + (10 + \text{Cavities})$	0.17
Beta	$12 \times 12 \times 12$	0.20
IM-5	?	0.13

Amorphous silica (Aerosil 200, Degussa), sodium aluminate (56% Al_2O_3, 37% Na_2O, Carlo Erba), sodium hydroxide (98% Prolabo), sodium bromide (99%, Scharlau), and water were used as reagents. The chemical composition of the synthesis gel was as follows:

$$60SiO_2 : 1.5Al_2O_3 : 17Na_2O : 6NaBr : 10R : 2400H_2O$$

The required amount of silica was added to a solution of the organic structure-directing agent in water with stirring. Then, a solution of sodium aluminate, sodium hydroxide, and sodium bromide in water was added and the mixture was stirred for 30 min. After 10 days of heating at 448 K, the autoclaves were quenched and the contents filtered and repeatedly washed with distilled water. The Si/Al ratio of the resulting sample, as determined by chemical analysis, was 16.

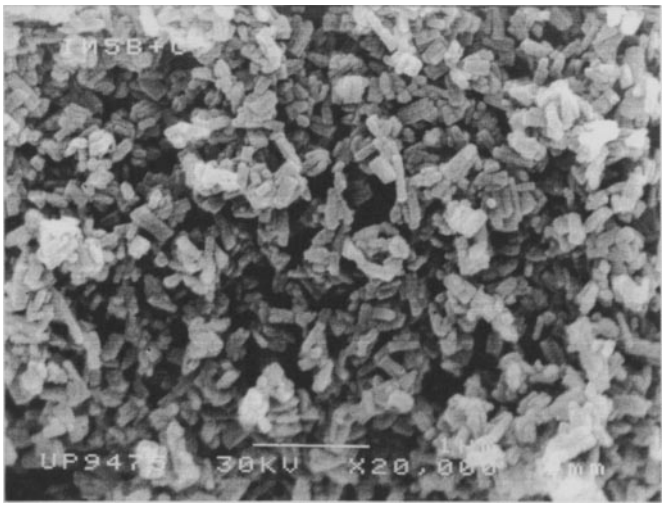

FIG. 2. Scanning electron microscopy image of the IM-5 sample.

Powder X-ray diffraction (XRD) data of the material were recorded in a Philips X'Pert MPD diffractometer equipped with a PW3050 goniometer (Cu $K\alpha$ radiation, graphite monochromator) provided with a variable divergence slit. The corresponding XRD patterns of the material in its as-prepared and acid form (see below) are presented in Fig. 1, and they correspond to a pure sample as described in (5). Scanning electron microscopy (SEM) using a JEOL 6300 microscope was also employed to characterise the zeolite. Figure 2 shows a SEM image of the IM-5 sample where defined crystals of $\sim$0.30 μm can be observed. For adsorption and catalytic testing the sample was calcined in air at 853 K for 3 h and exchanged twice with a solution of NH_4Cl followed by calcination at 773 K to obtain the zeolite in its

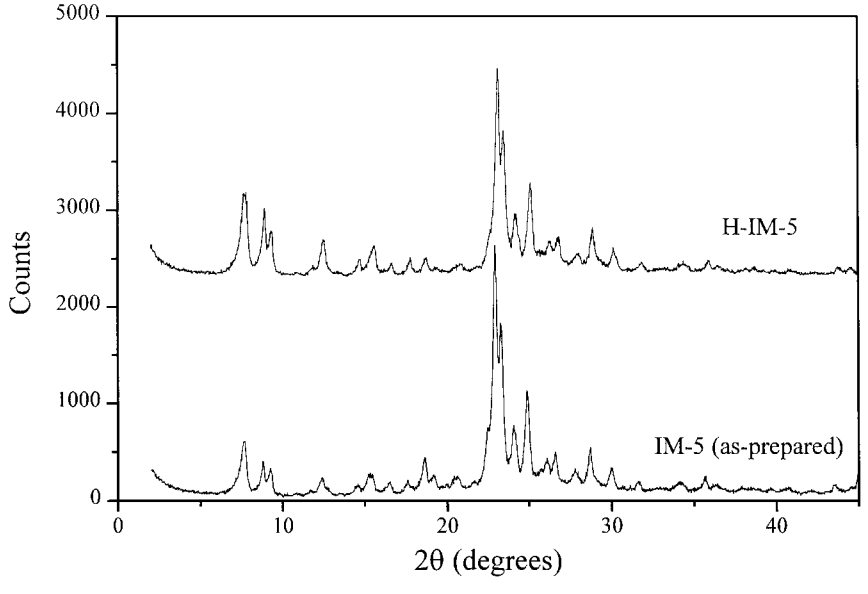

FIG. 1. X-ray diffraction patterns of zeolite IM-5 in its as-made and acid form.

acid form. For the *n*-decane test the sample was impregnated with 1 wt% of Pt. After impregnation the material was calcined at 773 K for 2.5 h and then pelletized in a particle size range of 0.59–0.84 mm. The pelletized catalyst was introduced in the reactor and after N_2 stripping at 773 K for 2 h was reduced "*in situ*" at 723 K with H_2 (300 cm^3 min^{-1}) for 2 h.

Catalytic Experiments

The hydroisomerization–hydrocracking of *n*-decane was carried out in a fixed-bed glass reactor at 413–463 K with a molar ratio of H_2 to decane of 100. The reaction products were analysed by GC-MS, using a 30-m long fused-silica capillary column. The level of conversion was varied by changing the reaction temperature but keeping constant the W/F at 0.52 h and the H_2/*n*-decane ratio at 100.

The *m*-xylene isomerization was carried out in a fixed-bed glass tubular reactor at 623 K and atmospheric pressure. The *m*-xylene/N_2 molar ratio was 0.25, and different conversion levels were obtained by varying the contact time between 0.06 and 0.20 g h mol^{-1}, following the protocol previously described (10). The accumulated liquid samples were analysed by GC using a 60-m long "supelcowax-10" capillary column. Initial selectivities were obtained from the initial rates of formation of the products. Initial rates were calculated from the initial conversions, X_0, by extrapolating the conversion, X, measured at different times-on-stream (t) according to the following equation:

$$X = X_0 \exp(-kt^{1/2}).$$

Adsorption Experiments

Amounts adsorbed were measured in a conventional volumetric apparatus as a function of pressure to obtain the volumetric isotherm. Reproducibility, determined by cumulative helium expansions, was always better than 0.2 μmol. A heat-flow microcalorimeter of the Tian-Calvet type (model BT, Setaram, France) coupled with the volumetric apparatus referred to above was used to determine the isosteric heat of adsorption, $q^{st,\sigma}$, as a function of the amount adsorbed, n^{σ}, to produce the differential calorimetric isotherm (11, 12). The detection limit of the calorimeter was about 0.2 mJ and the reproducibility of the measurements was in the order of 2 mJ.

Before each experiment the samples were heated in oxygen flow, ca. 30 cm^3 min^{-1} from room temperature up to 723 K, kept at this temperature for 2 h, and outgassed overnight at 723 K in a vacuum better than 1 mPa. Both isotherms, volumetric and calorimetric, were simultaneously determined as described in detail elsewhere (12, 13).

Postadsorption experiments and consecutive adsorption of a second adsorbate were performed after preadsorption of a first adsorbate and outgassing for a period of 30 min at the temperature of the experiment, unless otherwise stated. The amount of preadsorbate desorbed in this process was determined from the calorimetric desorption peak and from this the amount remaining adsorbed, n^{σ}_{irr}, was calculated (13).

Amounts adsorbed are expressed in millimole of molecules per gram of sample dried under vacuum at 723 K.

3. RESULTS AND DISCUSSION

Catalytic Tests

In Table 1 the pore volume of zeolites with 10 MR unidirectional channels (ZSM-48 and ZSM-22), 10×8 MRs (Ferrierite), bidirectional 10 MRs (ZSM-5), unidirectional 12 MRs, either circular (SSZ-24) or more elliptical (ZSM-12), connected 12 and 10 MRs (SSZ-26), 12 and 8 MR pores (Mordenite), or 12 MR tridirectional (Beta), as taken from the literature, are given, together with that of IM-5. The results show that from the standpoint of pore volume, IM-5 can hardly be identified as a 10×8, 10×6, or uni- or tridirectional 12 MR zeolite. Thus, to a first approximation one may postulate that this zeolite could be formed by a system of bidirectional 10 MRs, unidirectional 10 MR with lobes, or 12×10 MRs if the 12 MRs are very elliptical.

n-Decane Test

It was shown (7–9) that it is possible to gather more detailed information about the pore topology of zeolites by using test reactions in which intermediates and or products wit different sizes are being formed. Here, we selected the *n*-decane test (7), owing to its excellent track record with respect to the determination of zeolite pore structures. Martens *et al*. (7) reacted *n*-decane in the presence of zeolites of known topologies, and by a careful analysis of the reaction products, found eight independent criteria which could be used to estimate the pore topology of molecular sieves. The first criterium considers the ratio of dibranched to monobranched isomers obtained under conditions where the selectivity to isomers is maximum. Applying this criterium (see Fig. 3), the authors observed that large pore zeolites with large cavities gave dibranched-to-monobranched ratios close to 0.55, while zeolites with small pores and large cavities gave values between 0.33 and 0.05. Finally, the values for the dibranched/monobranched ratio with bidirectional zeolites are between 0.12 and 0.03.

When this criterium is applied to IM-5, the results, as given in Fig. 3 (7), show that this zeolite should have 12 MR pores, or 12 MR pores plus cages. However, when more detailed product analysis was carried out, Martens *et al*. (7) showed that a correlation between the constraint index CI^0 (2 MC_9/5 MC_9) and the 2,7-dimethyloctane concentration exists and can be used to differentiate between 12 and 10 MR pore zeolites. The results presented in Fig. 4 and Table 2 clearly show that the values for IM-5 fall in between those of ZSM-48 and FER. Taking into account that

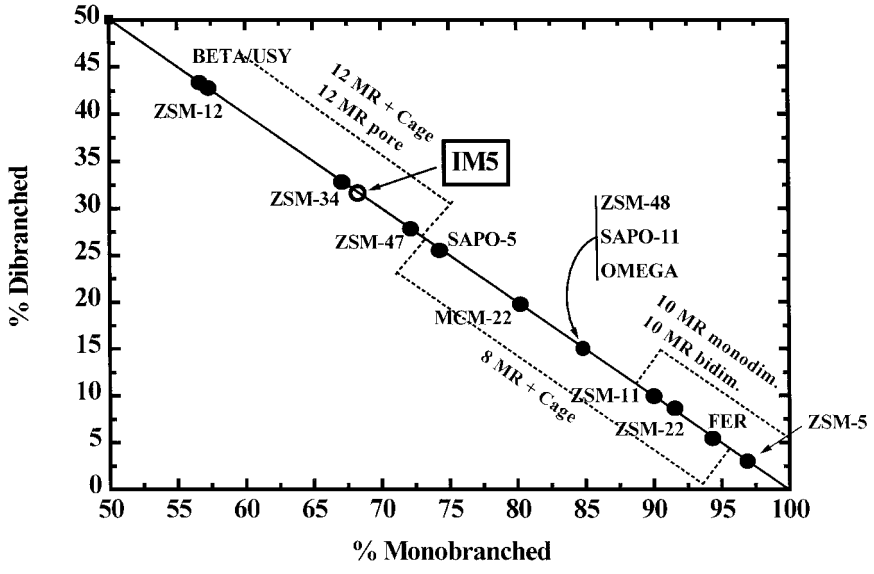

FIG. 3. Relative distribution of monobranched versus dibranched isomers in the *n*-decane test over different zeolites at maximum isomer conversion.

the yield of 2,7-dimethyloctane in this respect is independent of crystal size and morphology (7), we can say from the results in Table 2 that IM-5 is a 10 MR pore zeolite. Moreover, the presence of propylheptane in the isomers produced was used (7) as a fingerprint to show the presence of 12 MR pores. Since this isomer was not present in our products, we therefore concluded that IM-5 is formed by 10 MR pores.

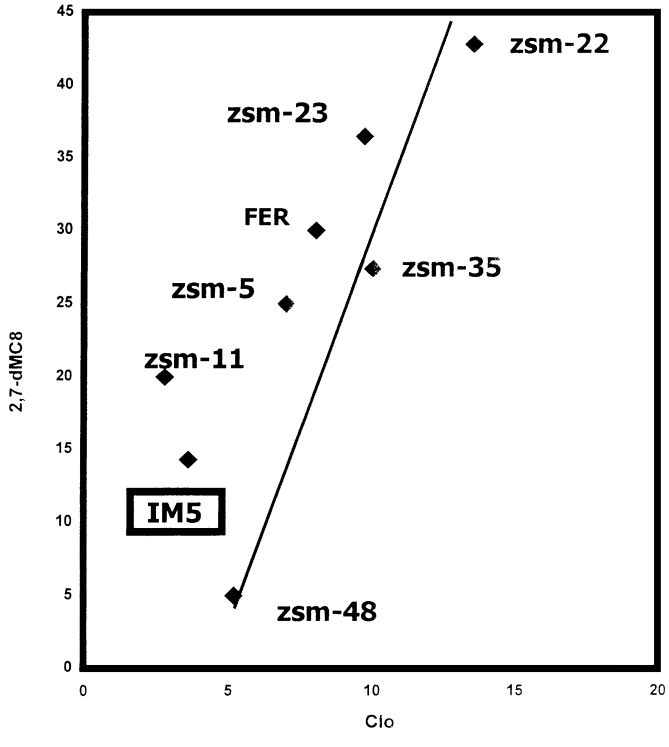

FIG. 4. 2,7-Dimethyloctane concentration versus the constraint index CI^0 ($2MC_9/5MC_9$).

Another criterium in the *n*-decane test takes into consideration the fact that ethyloctane isomers have a larger kinetic diameter than monomethyl-branched isomers. Therefore, the amount of ethyloctane formed among the monobranched products, when working at low levels of conversion (5%), can also differentiate between pores of different dimensions. Following this, the results given in Fig. 5 show that IM-5 behaves like Ferrierite, ZSM-5, ZSM-11, ZSM-48, or ZSM-22, indicating a behavior more typical of 10 MR zeolites. Furthermore, 4-ethyloctane was not present in the reaction products, this again indicating that product formation via propyl or butyl shifts must be restricted in IM-5 as a consequence of constraints in the pore diameter, which do not allow its formation and/or desorption. Taking this into account, we should conclude that this zeolite ought not have large 12 MR pores, or if they are present as suggested by the first criterium, they should be strongly hindered.

In the next criterium the relative kinetic diameter of the 2-methylnonane ($2MC_9$) and 5-methylnonane ($5MC_9$) is considered, and since the size of the former is smaller, the ratio of $2MC_9$ to $5MC_9$ should be affected by the dimension of the pores. From Fig. 6, it can be observed that the values obtained for IM-5 would indicate that strong restrictions exist over the pores to hinder the formation of the bulkier $5MC_9$. Once again, from this criterium one should conclude that the most probable pore topology involves 10 MR pores. However, from this criterion alone it is very difficult to completely exclude the presence of a strongly elliptical 12 MR pore.

TABLE 2

Distribution of 2,7-Dimethyloctane (2,7-dMC8) in the Dibranched Isomers at a Yield of 5%

Zeolite	Pore dimensions (nm)	Dimensionality of pores	Crystal shape and dimensions (μm)	2,7-dMC8 (mol%)
ZSM-22	0.55 × 0.45	1-D	0.1–0.5 × 1–2 (needles)	42
ZSM-23	0.56 × 0.45	1-D	—	37
ZSM-48	0.56 × 0.53	1-D	0.05 × 1 (needles)	14.8
IM5	**?**	**?**	**0.3 × 0.1 (rods)**	**14.2**
FER	0.55 × 0.43	2-D	—	28.3
ZSM-35	0.48 × 0.34	2-D	0.3 × 1 (Rods)	30
ZSM-11	0.55 × 0.51	2-D	1 (spherulitic)	20
ZSM-5	0.54 × 0.52	2-D	1–2 (monocrystals)	25
USY	0.74	3-D	—	8

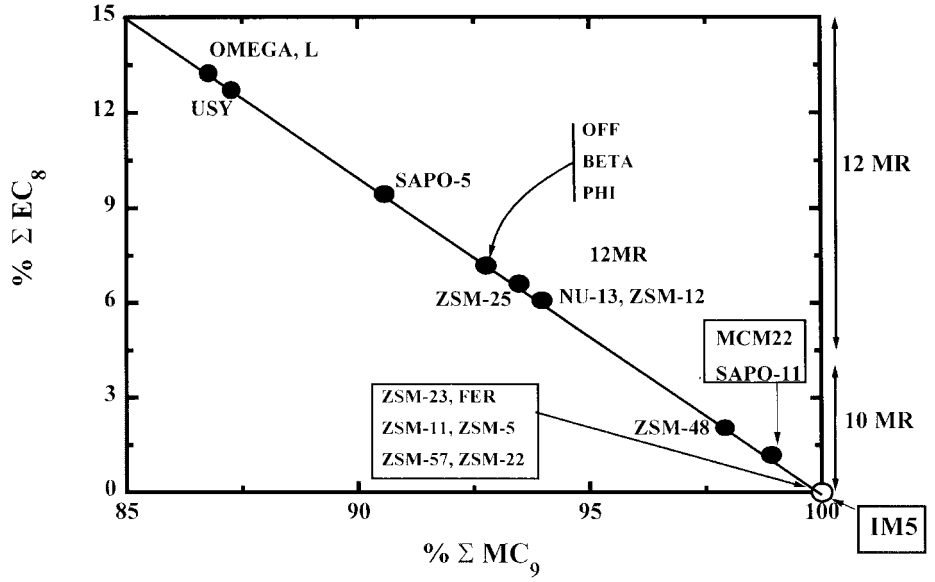

FIG. 5. Ethyloctane isomers (EC_8) versus methylnonanes (MC_9) in monobranched isomers at 5% conversion to isomers.

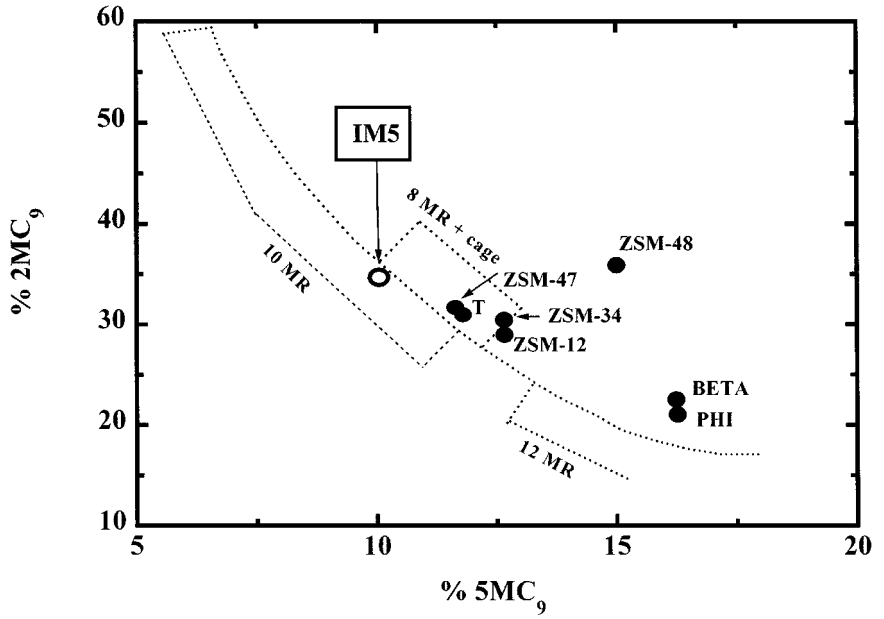

FIG. 6. Relative concentration of $2MC_9$ versus $5MC_9$ in monobranched isomers at 5% conversion to isomers.

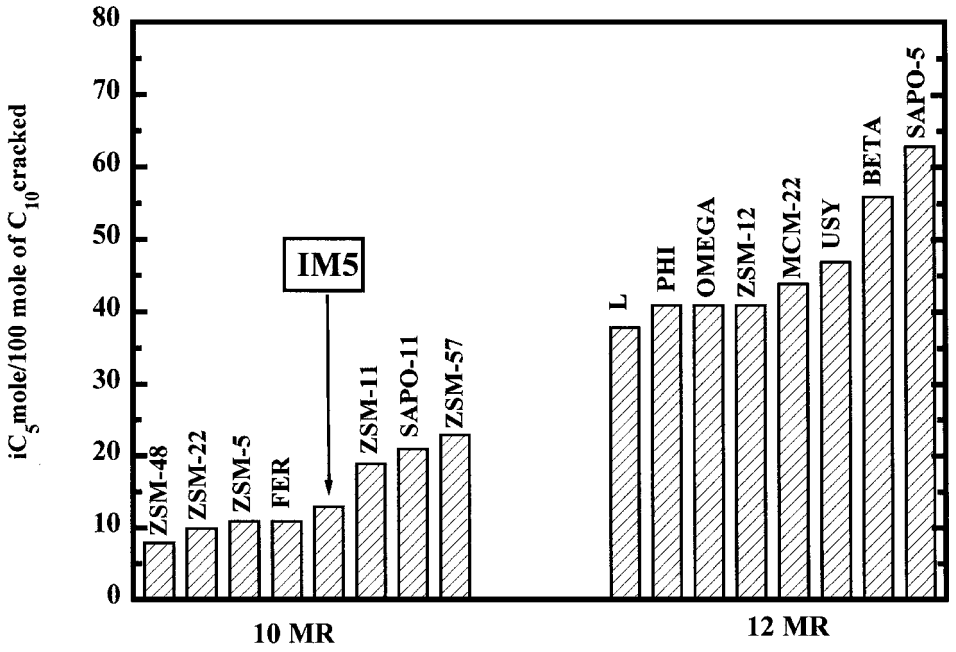

FIG. 7. Absolute yield of isopentane formed over different zeolites at 5% conversion to cracking.

In the next criterium, the authors considered (7) that in the hydrocracked products the formation of isopentane will require the most bulky intermediate branched carbocations, i.e., 3,5-dimethyloctane and 3,3,5-trimethylheptane. Then, zeolites that restrict the formation and/or desorption of these bulky intermediates will produce lower amounts of isopentane. The results from this test are given in Fig. 7 where it can be seen that IM-5 is located in the same position as ZSM-5, ZSM-11, or Ferrierite, again indicating that IM-5 probably consists of 10 MR pores.

At this point, it appears that, from a reactivity point of view, the pore topology of IM-5 behaved as if it was formed by a 10 MR. Also, from the first criterion it appeared that lobes or channel crossing might occur. Then, to be more specific with our assignment, we applied a second test reaction.

Xylene Isomerization–Disproportionation

The isomerization and disproportionation of xylenes was proposed as a test reaction which allows one to differentiate between 10 and 12 MR pores while indicating if there are lobes, cages, or crossing channels present (8). The basic principle used in this case is that during the isomerization of *m*-xylene, both *p*- and *o*-xylenes are formed. However, at low levels of conversion, 10 MR pore zeolites give higher para/ortho ratios (p/o) than 12 MR pore zeolites, owing to differences in the diffusion of both isomers through the narrow channels of the 10 MR zeolites (6). Moreover, if one recalls that the disproportionation of xylenes to trimethylbenzenes and toluene is a bimolecular reaction which involves a much bulkier reaction transition state than the monomolecular isomerization process (10), it is clear that the ratio of isomerization to disproportionation will give an indication of the presence of lobes, cavities, or crossing of pores where the available space will be large enough to allow the bimolecular reaction to occur.

Taking this into account, and comparing the initial para/ortho ratio obtained for zeolite IM-5 with other 10 MR and 12 MR zeolites of known structure (Figs. 8), it can be seen that IM-5 shows a high para/ortho value which is similar to the values found for 10 MR zeolites. It is then apparent that if any 12 MR pore exists, it should be highly deformed, giving final dimensions close to those of a 10 MR pore.

When the isomerization to disproportionation (i/d) ratios are considered (Figs. 9) it can be observed that IM-5 shows an intermediate behavior between that of 10 and 12 MR pore zeolites, where the i/d ratio is found to be higher than that of large pore structures, but lower than medium pore zeolites. The difference in the i/d ratio between 10 MR and 12 MR structures is attributed to the steric hindrance imposed in the former to the formation of any of the 1,1-diphenylmethane transition state complexes required to form the disproportionation products. This result indicates that even if IM-5 is formed by 10 MR pores, it should have larger internal voids which would be responsible for the relatively low i/d value found.

An additional selectivity parameter which can be highly informative with respect to the presence of internal cages, lobes, or channel crossings is the distribution of the trimethylbenzene (TMB) products formed by disproportionation of *m*-xylene. Indeed, this reaction occurs through the formation of three possible 1,1-diphenylmethane-type

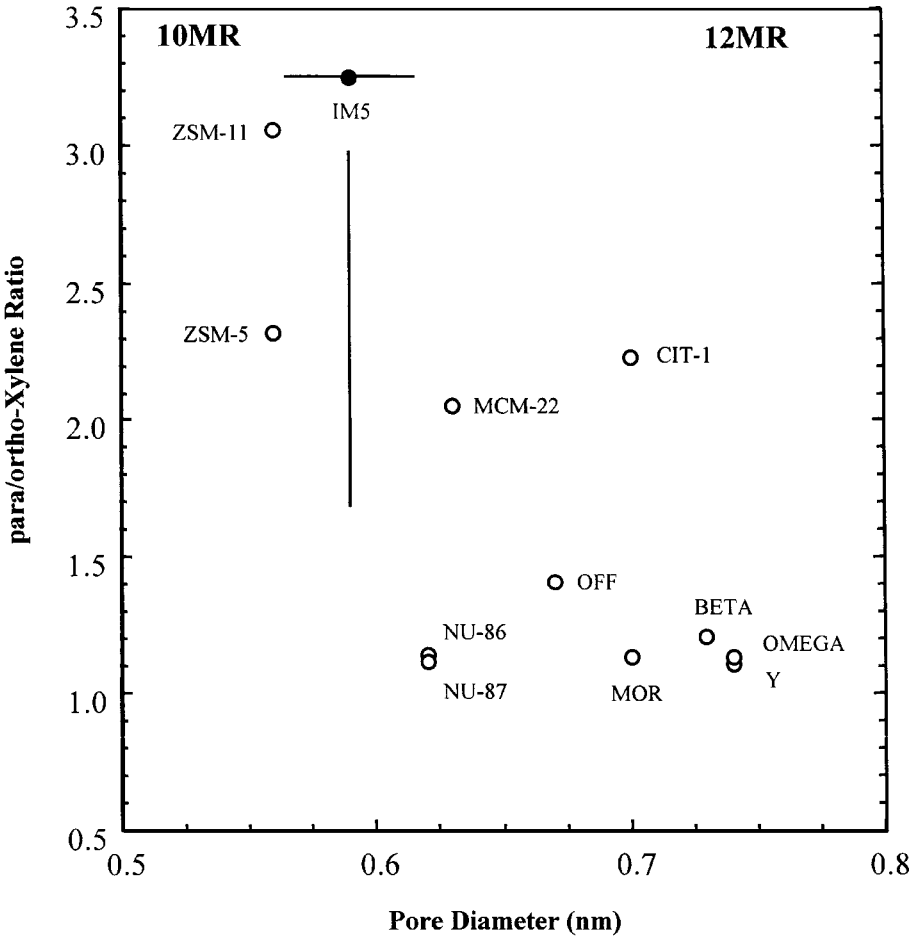

FIG. 8. Initial para/ortho ratio obtained in the isomerization of *m*-xylene on different zeolites of known structures and on IM-5. ZSM-5 was a commercial PQ sample (CBV5020) with Si/Al = 25 and crystallite size of 0.3–0.4 μm.

transition states (14, 15), leading to the formation of 1,2,4-, 1,3,5-, and 1,2,3-TMB isomers as schematised in Fig. 10.

A simple molecular modelling exercise shows that none of the three transition state complexes can be easily accommodated inside the pores of 10 MR zeolites, and when disproportionation occurs in small amounts, the less impeded complex III leading to 1,2,4-TMB should be favored. In Table 3 the distribution of the TMB isomers obtained on zeolite IM-5 at low levels of *m*-xylene conversion is compared with that obtained on other 10 and 12 MR zeolites, indicating that complexes I and II can hardly be accommodated within the pores of this zeolite. However, at conversions of about 10%, 1,3,5-TMB and 1,2,3-TMB are detected in the disproportionation products on IM-5. Meanwhile, these isomers are not formed on ZSM-5 at conversions as high as 17 mol%.

This could reflect the presence of larger void spaces in IM-5 than in ZSM-5. It should be taken into account that the results are not masked by the reaction at the external surface since the crystallite size of IM-5 and the ZSM-5 used is very similar.

Then, we could explain the selectivity pattern of IM-5 for the reactivity of *m*-xylene, assuming that this zeolite is formed by 10 MR pores with void volumes larger than those due to the channel crossing in ZSM-5. Possible structures consistent with this topology and which are also consistent with the results from the *n*-decane test are as follows:

—a bidirectional structure formed by 10 MR pores;
—unidirectional 10 MR with lobes.

4. ADSORPTION RESULTS

Adsorption of n-Hexane

The differential calorimetric isotherm, $q^{st,\sigma} - n^{\sigma}$, of *n*-hexane on the IM-5 zeolite is shown in Fig. 11. The same results were obtained at 315 and 330 K, indicating that under the experimental conditions used here there are no diffusional restrictions. The adsorption heat of *n*-hexane remains practically constant up to ca. 0.99 mmol g^{-1}, before a steady decline reflecting the completion of micropore filling begins. The packing density found in the micropores

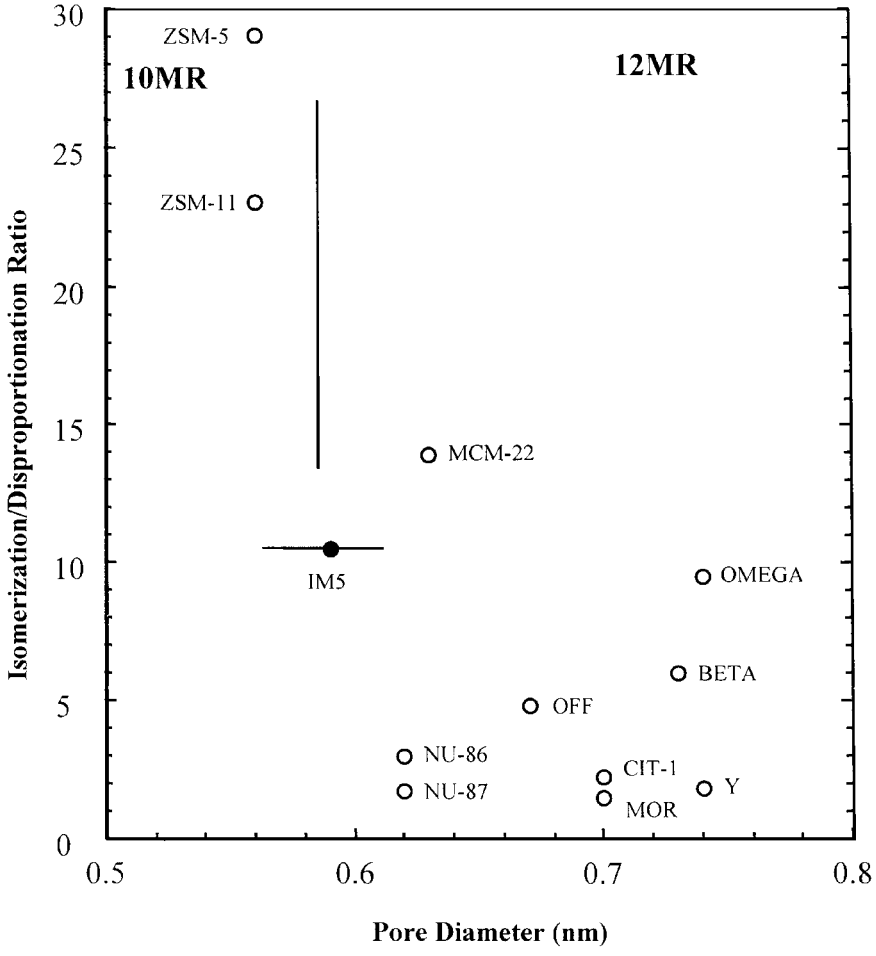

FIG. 9. Initial isomerization/disproportionation ratio in the *m*-xylene test obtained on different zeolites of known structure and on IM-5. ZSM-5 was a commercial PQ sample (CBV5020) with Si/Al = 25 and crystallite size of 0.3–0.4 μm.

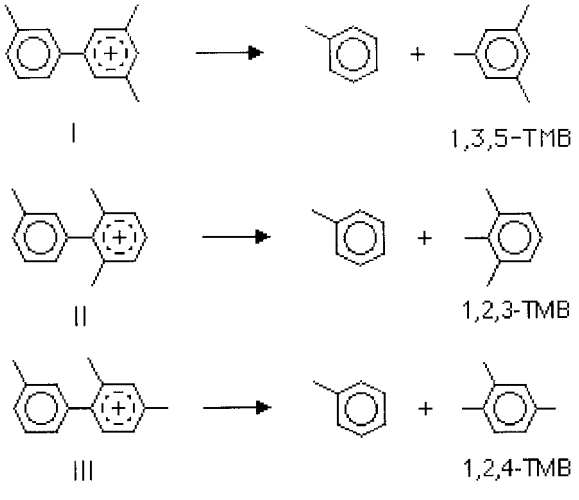

FIG. 10. Possible transition state complexes for the disproportionation of *m*-xylene.

is 7.5 mmol cm^{-3}, which is slightly higher than the liquid molar density of *n*-hexane at 315 K (7.42 mmol cm^{-3}). A close agreement between the two density values is normally found in large pore zeolites, and only occasionally in medium and small pore zeolites. However, caution must be applied in using this as a differentiation criterion, since also in medium pore zeolites such as ZSM-5 (16, 17) and ZSM-11 (13) a close packing of *n*-hexane exists which gives similar values for the packing density in the micropores and the density of *n*-hexane at the adsorption temperature. Thus, we can say that the similar density values found in the IM-5 sample may probably be due to an unusual size and shape fitting of *n*-hexane to the geometrical characteristics of the micropores.

Toluene Adsorption

In the case of toluene, the shape of the calorimetric thermograms indicates that at 315 K the process is controlled by diffusion. Correspondingly, points measured at

TABLE 3

Distribution of Trimethylbenzenes at Low Conversions of *m*-Xylene on Different Zeolites

Zeolite	Conversion	Trimethylbenzene (%) 1,3,5-	1,2,4-	1,2,3-	1,2,3/1,3,5 ratio
10 MR					
ZSM-48[a]	5.4	0.0	100.0	0.0	—
	15.1	10.4	89.6	0.0	0.0
ZSM-5[b]	9.7	0.0	100.0	0.0	—
	17.1	0.0	100.0	0.0	—
IM5	8,1	4.4	95.6	0.0	0.0
	12,3	6,1	89.9	4.0	0.66
	18.9	6.0	90.3	3.8	0.63
10 MR + 12 MR					
MCM-22[c]	7.5	0.0	100.0	0.0	—
	10.8	21.1	78.9	0.0	0.0
	17.8	20.7	79.3	0.0	0.0
CIT-1	15.7	16.3	76.3	7.4	0.45
NU-87	12.8	1.4	94.0	4.6	3.3
NU-86	8.8	18.1	75.2	6.7	0.37
12 MR					
FAU[a]	7.2	28.1	64.0	7.9	0.28
BETA[a]	8.9	22.6	73.1	4.2	0.19
MOR[a]	6.3	19.2	71.7	9.1	0.47
	10.6	21.3	69.9	8.8	0.41
OMEGA[a]	7.4	13.6	77.4	9.0	0.66
	8.6	10.0	81.3	8.7	0.87
OFF[a]	6.7	0.0	95.3	4.7	∞
	12.2	0.0	94.9	5.1	∞

[a] Ref. (8).
[b] Commercial PQ sample (CBV5020) with Si/Al = 25 and crystallite size of about 0.3–0.4 μm.
[c] Ref. (9).

this temperature are low (points 1–7 in Fig. 12). However, when the temperature was increased to 330 K, the diffusion limitations disappeared (Fig. 12). Note that differences observed at 330 and 365 K are negligible. Nevertheless, at 365 K the equilibrium is already slightly displaced toward desorption, and consequently only the results at 330 K were considered here.

Toluene differential calorimetric isotherms show an initial decrease in the heat of adsorption up to 0.27 mmol g^{-1}. This is a clear indication of the existence of a specific interaction between toluene and certain sites in the zeolite walls. In the curve (Fig. 12) a small maximum can also be observed before the final decrease in the heat of adsorption occurs. This feature can give specific information on the pore geometry since it is ascribed to the presence of lateral interactions inside wider spaces such as cavities, side pockets, or crossing of channels (13, 16, 18–20).

From the toluene uptake on the micropores (0.87 mmol · g^{-1}) a packing density of 6.6 mmol cm^{-3} was calculated, which is well below the molar density of liquid toluene at 330 K (9.04 mmol cm^{-3}). This result indicates the difficulty of accommodating toluene molecules inside micropores of small diameter (13).

m-Xylene Adsorption

The $q^{st,\sigma} - n^{\sigma}$ curve of *m*-xylene adsorption at 350 K (Fig. 13) is qualitatively similar to that of toluene, but the amount of *m*-xylene adsorbed in the micropores (0.68 mmol g^{-1}) is some 20% lower than that for toluene. This is due to the larger size of the *m*-xylene molecules which occupy more space and have more problems packing closely. This is consistent with the much lower packing density of *m*-xylene (5.2 mmol cm^{-3}) inside the pores with respect to the density of liquid *m*-xylene at 350 K (7.68 mmol cm^{-3}). The initial decrease in the heat of adsorption observed from the toluene experiments is also apparent here, up to 0.29 mmol g^{-1}, a value similar to that of toluene.

A very small amount of mesitylene (1,3,5-trimethylbenzene) was adsorbed on IM-5 and it was seen clearly that no adsorption occurred in the micropores.

The adsorption of the alkyl aromatic hydrocarbons was quite instructive from the point of view of rationalising the pore geometry. Indeed, the fact that *m*-xylene can diffuses while mesitylene does not indicates that the structure does not contain 12 MR pores, or if they are present, they should be constructed in such a way to not permit the diffusion of trimethylbenzene. Then, if one is left with 10 MR pores, the fact that toluene already displays some diffusional problems at 315 K but *m*-xylene, which has a larger size, diffuse reasonably well at 330 K, suggests that the 10 MR micropores are not completely circular or that they have some sinusoidal character.

Moreover, from the total amounts of hydrocarbons adsorbed as well as from the micropore volume determined by N_2 adsorption (Table 1), we can see that the pores cannot be unidirectional; therefore, we expect either lobes or channel crossing to exist. This was supported by the presence of a small maximum near the completion of micropore filling in the *n*-hexane and toluene adsorption isotherms (Figs. 11 and 12). We know from a study of existing structures that "wider spaces" within zeolites may take various forms, including the presence of channel intersections, lobes, or side pockets, or even the presence of 12 MR pores connecting 10 MR pores as in the case of zeolite NU-87. We have investigated a sample of NU-87 prepared following (2), which has a Si/Al ratio of 20, a crystallite size of 0.2 μm, and a pore volume of 0.16 cm^3 g^{-1} instead of 0.13 cm^3 g^{-1} as in IM-5. Moreover, the p/o and i/d ratios obtained during the isomerization of *m*-xylene are 1.1 and 1.7 respectively for NU-87, while they are 3.0 and 9.7 for IM-5. Therefore, we can rule out the possibility of a pore topology formed by 10 MR pores connected by 12 MR pores in IM-5. Thus, we are left with the following possibilities:

—a bidirectional system of 10 MR crossing pores;
—10 MR channels with lobes

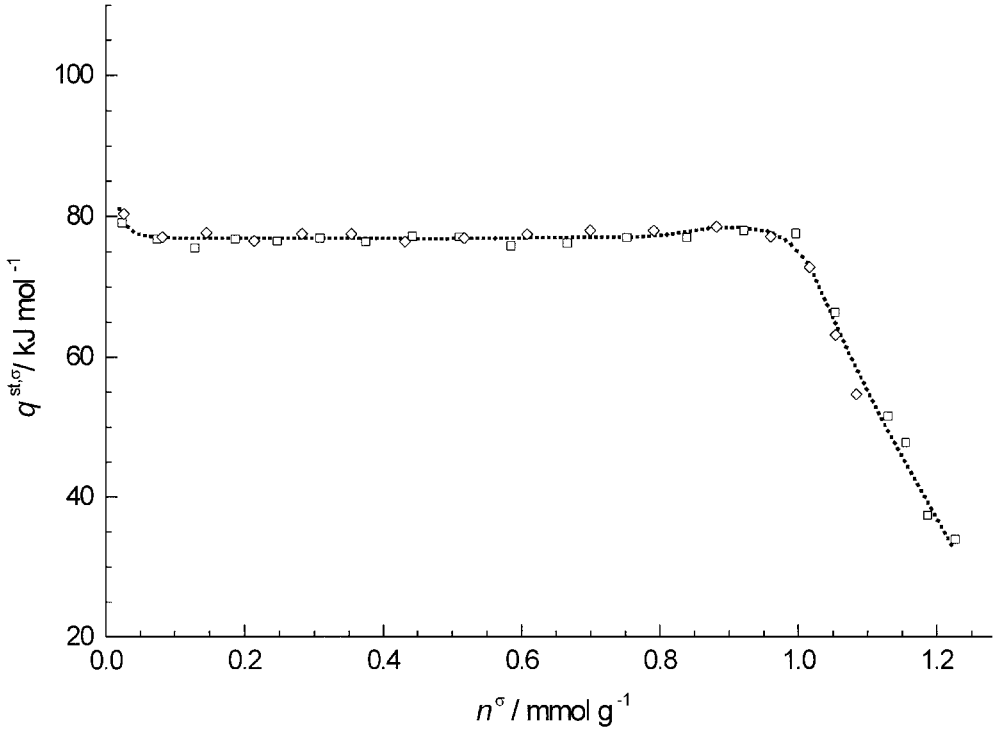

FIG. 11. Differential calorimetric adsorption isotherms of *n*-hexane on zeolite IM-5 at 315 K (□) and 330 K (◇).

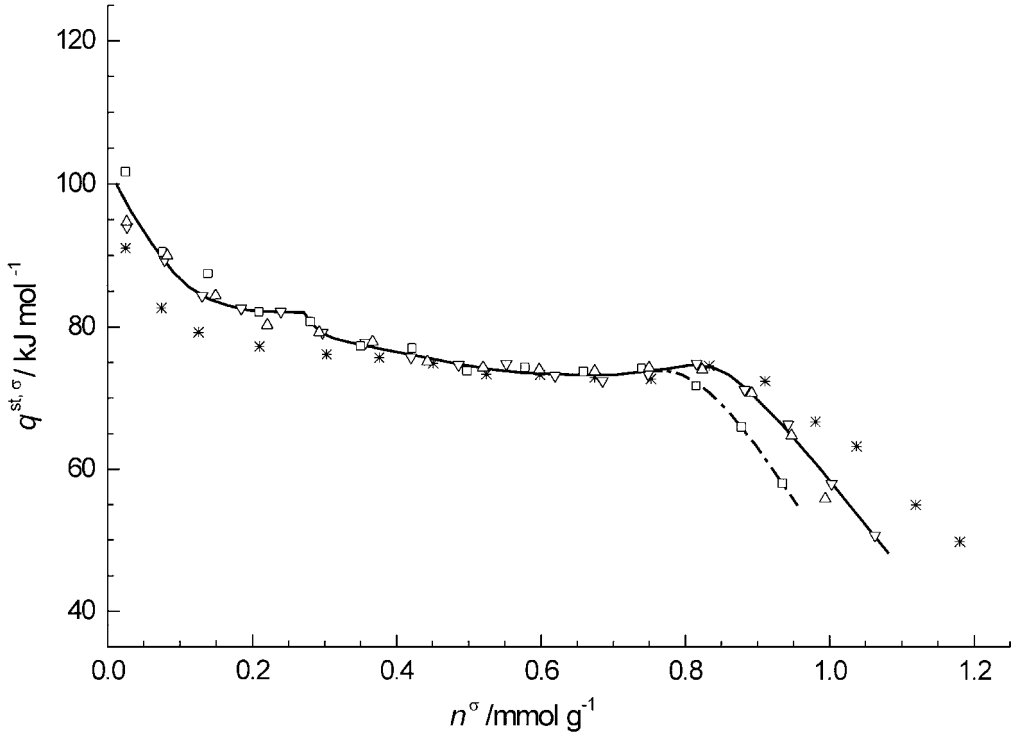

FIG. 12. Differential calorimetric adsorption isotherms of toluene on zeolite IM-5 at 315–330 K (*), 330K (△, ▽), and 365 K (□).

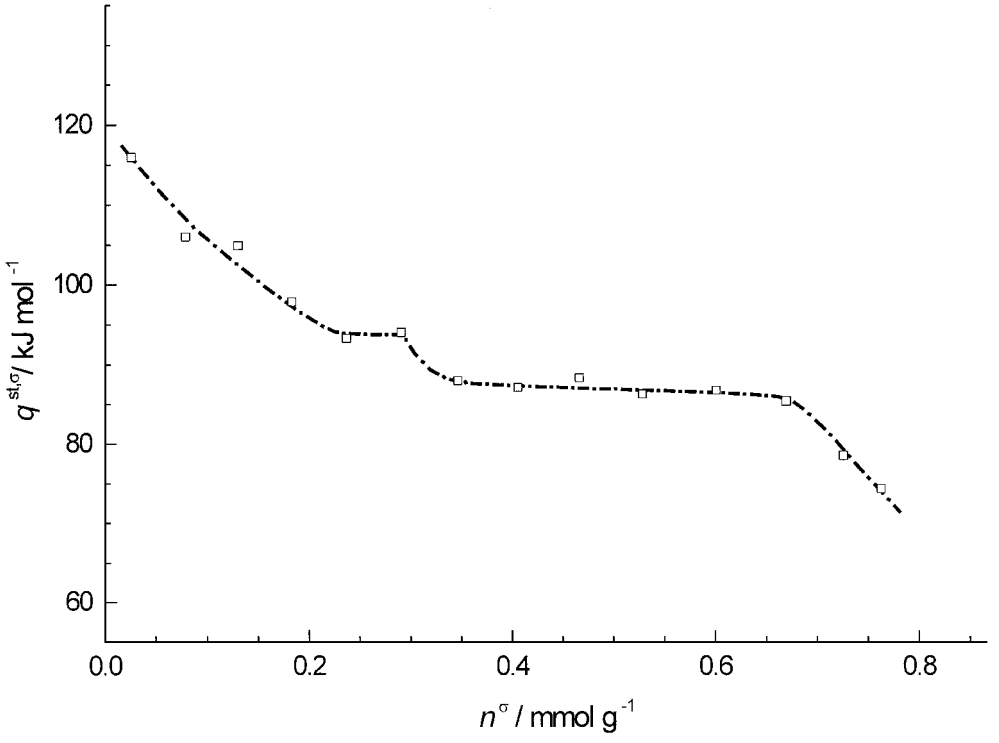

FIG. 13. Differential calorimetric isotherms of *m*-xylene on zeolite IM-5 at 350 K (□).

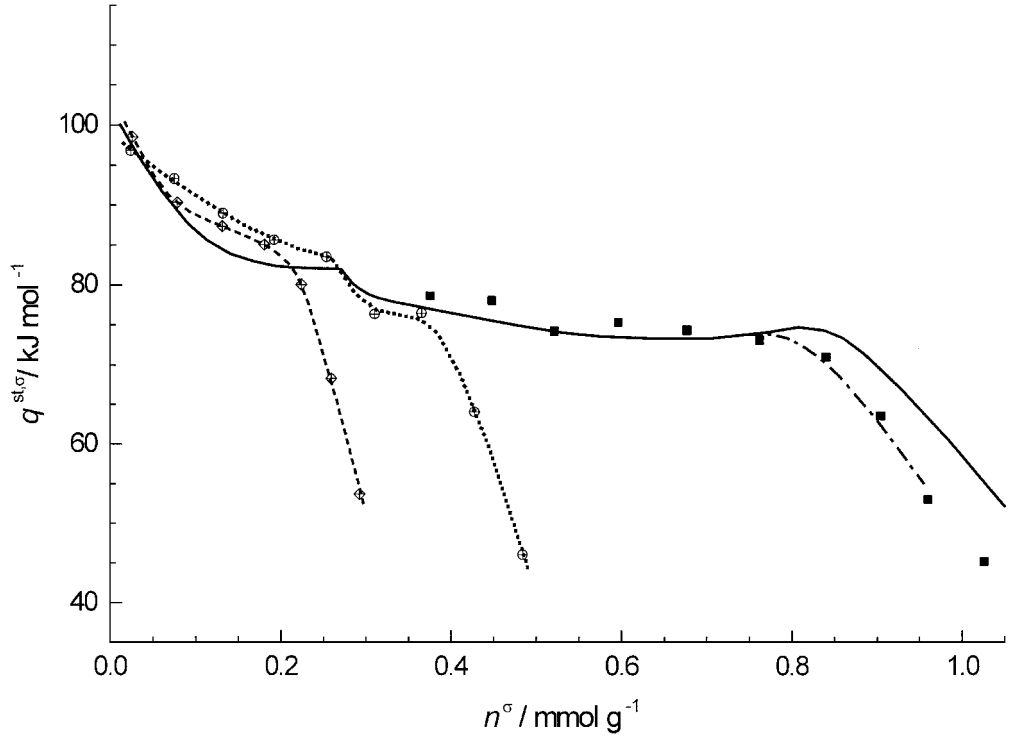

FIG. 14. Differential calorimetric postadsorption isotherms on zeolite IM-5 of toluene at 365 K after preadsorption of toluene at 365 K, displaced to the right-hand side, 0.34 mmol g^{-1} (amount remaining on the sample after the intermediate outgassing) (■); toluene at 330 K after preadsorption of *n*-hexane at 330 K (⊕); and toluene at 330 K after preadsorption of cyclohexane at 330 K (⊕). Toluene $q^{st,\sigma} - n^{\sigma}$ adsorption curves on the clean sample at 330 K (—) and 365 K (- · · · -).

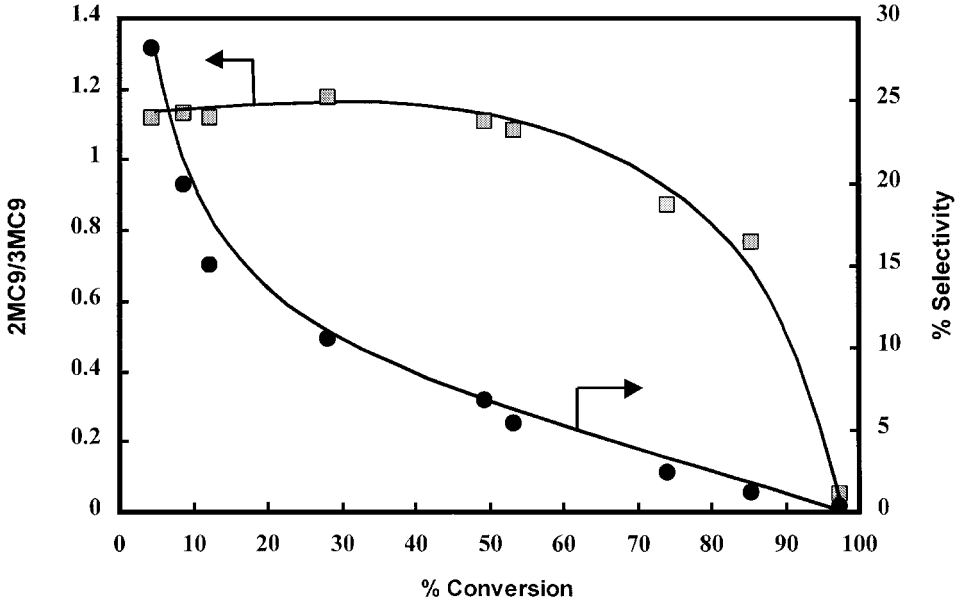

FIG. 15. Selectivity and $2MC_9/3MC_9$ ratio versus conversion in the *n*-decane isomerization reaction.

To further discuss these possibilities, we carried out postadsorption of an adsorbate after preadsorbing of another one.

Postadosorption of Toluene

A blank experiment is carried out by postadsorption of toluene, after toluene was preadsorbed and outgassed at 365 K. The results in the form of a differential calorimetric isotherm at 365 K are given in Fig. 14. They clearly demonstrate that intermediate outgassing simply removes a certain amount of toluene that was later readsorbed on the same adsorption sites, during the subsequent postadsorption experiment.

In a second set of experiments, a differential calorimetric isotherm at 330 K of toluene postadsorption after *n*-hexane preadsorption and outgassing at 330 K is carried out (Fig. 14). The amount of *n*-hexane remaining in the sample is 0.80 mmol g^{-1}, i.e., 81% of the micropore capacity for *n*-hexane. Thus, when toluene was postadsorbed, the results indicated that this is adsorbed on the most energetic sites. In fact, the toluene postadsorption differential calorimetric isotherm is virtually coincident with the isotherm of toluene on the most energetic sites in the clean sample (Fig. 14). It has to be noticed, however, that the heats of adsorption for toluene in the postadsorption experiment are somewhat higher because of the interaction with the preadsorbed *n*-hexane molecules. Similar results are found for toluene postadsorption at 330 K after cyclohexane preadsorption and outgassing at 330 K (Fig. 14). Taking into account the above results, it appears that postadsorbed toluene has to displace *n*-hexane and cyclohexane molecules from the most energetic sites. This implies that some counter diffusion of toluene–alkane has to occur. Clearly, this would be easier if a bidirectional system of crossing micropores with wide intersections exists or, if a unidirectional pore system were present, this should have large lobes which would also leave wider spaces within the channels to permit counter diffusion.

It is well known that unidirectional 10 MR zeolites with small (Ferrierite) or without (ZSM-22) side pockets, are good isodewaxing catalysts giving high selectivities to mono- and dibranched paraffins. In an analogous way, SAPO-11, which has elliptical unidirectional channels (dimensions 0.63×0.34 nm), is also a good catalyst for the isodewaxing of paraffins. Both materials give mainly 2-methylheptane when *n*-octane is isomerized (21).

On the other hand, a 10 MR bidirectional zeolite such as ZSM-5 is less selective to isomerization, giving more cracking and lower selectivity to the 2-methylhepatane, during *n*-octane hydroisomerization.

In this work, we have performed the hydroisomerization of *n*-decane and the selectivity curves, and the ratios of 2- to 3-methylnonane are given in Fig. 15. It can be seen there that IM-5 has a lower selectivity to isomerization, giving significant amounts of cracking. In this respect, the behavior of IM-5 is much more like ZSM-5 than Ferrierite or SAPO-11. Meanwhile, the ratio of 2- to 3-methylnonane is lower in the case of IM-5 and ZSM-5 than in the unidirectional 10 MR molecular sieves. This suggests that the pore topology of IM-5 would correspond better with a bidirectional system of 10 MR crossing channels. The adsorption results discussed compelled us to postulate that wider spaces in the form of either unidirectional flattened 10 MR channels or,

better, in the intersections of two sets of 10 MR micropores must be present in IM-5.

4. CONCLUSIONS

By combining catalytic tests and adsorption of hydrocarbons with different sizes and shapes, we suggest that the recently synthesised IM-5 zeolite could present a pore topology formed by either 10 MR crossing pores or 10 MR pores with lobes. The pore diameter should be close to but somewhat smaller than 5.5 Å. This type of topology offers interesting shape-selective catalytic properties that should, in some cases, be close to those of ZSM-5.

REFERENCES

1. Zones, S. I., Santilli, J. N., Ziemer, J. N., Holtermann, D. L., Pecorano, T. A., and Innes, R. A., PCT/US89/01179, 1989.
2. Casci, J. L., EP377291, 1989, Casci, J. L., Lake, I. J. S., Maberly, T. R., U.S. Patent 5041402, 1991; Shanon, H. D., Casci, J. L., Cox, P. A., and Andrews, S. J., *Nature* **353**, 417 (1991).
3. Leonowicz, M. E., Lawton, J. A., Lawton, S. L., and Rubin, M. K., *Science* **264**, 1910 (1994).
4. Casci, J. L., EP 463768A2, (1991); U.S. Patent 5108579 (1992).
5. Benazzi, E., Guth, J. L., and Rouleau, L., PCT WO 98/17581, 1998.
6. Csicsery, S. M., *Zeolites* **4**, 202 (1984).
7. Martens, J. A., Tielen, M., Jacobs, P. A., and Weitkamp, J., *Zeolites* **4**, 98 (1984); Martens, J. A., and Jacobs, P. A., *Zeolites* **6**, 334 (1986).
8. Gnep, N. S., Tejada, J., and Guisnet, M., *Bull. Soc. Chim. Fr. I* 5 (1982); Olson, D. H., and Haag, W. O., *ACS Symp. Ser.* **248**, 275 (1984); J. A. Martens, J. Pérez-Pariente, E. Sastre, A. Corma, and P. A. Jacobs, *Appl. Catal.* **45**, 85 (1988).
9. Corma, A., Corell, C., Llopis, F., Martínez, A., and Pérez-Pariente, J., *Appl. Catal. A* **115**, 121 (1994).
10. Corma, A., Llopis, F., and Montón, J. B., *J. Catal.* **140**, 384 (1993).
11. Guil, J. M., Pérez-Masiá, A., Ruiz-Paniego, A., and Trejo Menayo, J. M., *J. Chem. Thermodynam.* **26**, 5 (1994).
12. Guil, J. M., Pérez-Masía, A., Ruiz-Paníego, A., and Trejo Menayo, J. M., *Thermochim. Acta* **312**, 115 (1998).
13. Guil, J. M., Guil-López, R., Perdigón-Melón, J. A., and Corma, A., *Microporous Mesoporous Mater.* **22**, 269 (1998).
14. Santilli, D. S., *J. Catal.* **99**, 327 (1986).
15. Xiong, Y., Rodewald, P. G., and Chang, C. D., *J. Am. Chem. Soc.* **117**, 9427 (1995).
16. Wu, P., Debebe, A., and Ma, Y. M., *Zeolites* **3**, 118 (1983).
17. Parrillo, D. J., and Gorte, R. J., *J. Phys. Chem.* **97**, 8786 (1993).
18. Corma, A., Corell, C., Pérez-Pariente, J., Guil, J. M., Guil-López, R., Nicolopoulos, S., González-Calbet, J., and Vallet-Regí, M., *Zeolites* **16**, 7 (1996).
19. Sach, H., Jänchen, J., Thamm, H., Stiebitz, E., and Vetter, R. A., *Adsorption Sci. Technol.* **3**, 261 (1986).
20. Eder, F., and Lercher, J. A., *J. Phys. Chem.* **101**, 1273 (1997).
21. Miradieu, P., Tuan, V. A., Nghiem, V. T., Lai, S. Y., Hung, L. N., and Naccache, C., *J. Catal.* **169**, 55 (1997).